RSC Sustainability

PAPER

View Article Online
View Journal | View Issue

Cite this: *RSC Sustainability*, 2023, **1**, 574

A polysulfide-functionalized separator enables robust long-cycle operation of lithium-metal batteries†

Mengqiu Yang,[a] Yuanpeng Ji,[a] Yunfa Dong,[b] Shijie Zhong,[b] Haodong Xie,[b] Yuanpeng Liu,[b] Caomeng Zhang,[b] Sue Hao,[ac] Chunhui Yang,[ac] Jiecai Han[b] and Weidong He *[bde]

A separator plays an irreplaceable role in controlling battery safety and lifespan. Polyethylene (PE) and polypropylene (PP) are applied in batteries as separators to block electrons and transport lithium ions, on account of their chemical and mechanical stability. Unfortunately, the poor wettability and thermal stability limit their large-scale applications. Herein, a stable 16 μm PE-based separator was elaborately designed. The PESV composite separator was obtained by impregnating PE into the matrix of polysulfide (PSU) and polyvinylidene fluoride (PVDF). The obtained PESV showed higher porosity and uniform pore distribution with PSU and PVDF filling in the pores of PE. The PE skeleton provided chemical stability, and PSU offered robustness, while PVDF contributed to excellent wettability and thermal stability simultaneously. Thus, the PESV maintained morphology integrity at 150 °C while PE shrank at 60 °C. PESV exhibited a contact angle of 20° while PE was 48°, PESV reached 145 MPa while PE reached only 78 MPa. The robust PSU enabled the PESV composite separator with stable and long-term operation in the Li/Li battery, without obvious dendrites for nearly 1000 h, while the Li/Li battery with PE failed to handle it after 400 h at 0.5 mA cm^{-2}. Meanwhile, the LFP/Li batteries with the PESV reached a discharge capacity of 91 mA h g^{-1}, which retained 63% after 1000 cycles at 1C (1.28 mA cm^{-2}) with a mass loading of 4 mg cm^{-2}, demonstrating the stable cycling of LMBs with the PESV composite separator.

Received 24th December 2022
Accepted 28th February 2023

DOI: 10.1039/d2su00147k

rsc.li/rscsus

Sustainability spotlight

For the sustainable development of society, energy storage technology has become a key research topic, portable and rechargeable LIBs (electrochemical energy storage) greatly facilitate people's lives. A separator affects the transmission of Li^+ and plays a crucial role in LIBs. The poor wettability and thermal stability limit the large-scale applications of PP and PE separators. Herein, an ultra-stable PE-based separator (PESV) was designed by impregnating PE into the matrix of polysulfide and polyvinylidene fluoride. PSU offers robustness, while PVDF contributes to excellent wettability. Remarkably, the strong binding energy between PSU and Li^+ is responsible for the uniform distribution of Li^+. Our work aligns with the following UN sustainable development goals: affordable and clean energy (SDG 7), industry, innovation, and infrastructure (SDG 9).

1. Introduction

High capacity, high safety, and low-cost lithium metal batteries are urgently needed with the rapid development of electronic devices.[1–6] Separators may not be the active component of the battery, but influence the batteries' lifespan, cost, and safety.[7–10] Various factors, such as material, pore structure, porosity, tensile strength, Gurley value, thermal stability, wettability, and thickness of separators have impressive effects on the performance of batteries.[11] Significantly, the thickness of the separator has been widely discussed recently.[12] From one point of view, thin separators in batteries accommodate the volume change of the battery during the process of charging and discharging. From another perspective of sustainable development, the thin separators will cut the cost to some extent under

[a]*MIIT Key Laboratory of Critical Materials Technology for New Energy Conversion and Storage, School of Chemistry and Chemical Engineering, Harbin Institute of Technology, Harbin 150080, China*

[b]*National Key Laboratory of Science and Technology on Advanced Composites in Special Environments, Center for Composite Materials and Structures, Harbin Institute of Technology, Harbin 150080, China. E-mail: weidong.he@hit.edu.cn*

[c]*State Key Laboratory of Urban Water Resource and Environment, Harbin Institute of Technology, Harbin 150080, China*

[d]*Chongqing Research Institute, Harbin Institute of Technology, Chongqing 401151, China*

[e]*School of Mechanical Engineering, Chengdu University, Chengdu, China*

† Electronic supplementary information (ESI) available. See DOI: https://doi.org/10.1039/d2su00147k

the premise of being mechanically robust, showing the potential to be widely used in next-generation lithium batteries.[13–17] In addition to the thickness, the thermal stability of the separator is also one of the determining factors controlling the safety of batteries.[18,19] Temperature rises as the heat accumulates during the cycling of the batteries. Excessive temperature may cause the separators to shrink or even melt, which could cause severe safety incidents.[20,21] Heat-resistant ceramic materials have recently been incorporated into the separators to enhance the thermostability of composite separators such as Al_2O_3, SiO_2, and TiO_2.[13,22–24] The doping of these ceramic particles does enhance the thermal stability of the composite separators to a certain extent. Unfortunately, it increases the cost and volume of the battery dramatically, not to mention the sharp decline in discharge capacity caused by the incompatibility between the ceramic and electrolyte.[25]

The state-of-the-art functions of the separators in the batteries are absorbing the electrolyte and transferring the Li^+.[12,26–28] Therefore, the wettability between the separator and electrolyte plays a crucial role in battery cycling.[29,30] Good wettability can increase the electrolyte absorptivity and reduce the impedance in transferring Li^+. PE and PP are used as commercial separators in conventional batteries due to their chemical stability and sufficient mechanical strength.[20] However, hydrophobicity and poor thermal stability are still stumbling blocks to their further large-scale applications, as also the unstable and unsafe factors of the batteries. There are two main aspects of improving separator performances: (i) one is the modification of the traditional polyolefin separators. Organic/inorganic materials are coated or grafted on the surface of polyolefin to fabricate the composite separators. Zhu and coworkers[24] grafted TiO_2 on PE properly to form a composite separator with upgraded thermal stability, and Zhao *et al.*[19] coated nano-SiO_2 on both sides of PE to improve the heat resistance. (ii) The other is to find novel materials or new structures suitable for separators. Kong and coworkers[31] *in situ* synthesized the SiO_2@(PI/SO_2) hybrid separator showing robustness, high wettability, and fire resistance. Liu *et al.*[13] prepared scalable, safe, and high-rate supercapacitor separators based on PVDF. Guo and coworkers[32] designed a composite separator based on cellulose, which had good wettability with electrolytes for lithium-ion batteries. Wang's group[33] prepared a ZrO_2/PVDF-HFP composite separator for improving the safety of LIBs. Polyolefin-based separators showed high mechanical strength and chemical stability with improved thermal stability after coating or grafting heat-resistance materials. Apart from these, the low-cost additives make the composite separator suitable for mass production.[27,34] Nevertheless, separators based on the new materials still face a huge challenge: they cannot meet all the desired properties of the separators simultaneously.[35,36]

Here, an ultra-stable 16 μm PESV separator was rationally designed by impregnating PE into the matrix of PSU and PVDF. The higher porosity of 65% and uniform pore distribution were observed in PESV after PSU and PVDF filling in the pore of PE, resulting in higher electrolyte absorptivity for PESV than PE. The robust, thermal stable PSU and hydrophilic PVDF enabled PESV to show improved mechanical strength, upgraded wettability, and thermal stability. Assembled with the PESV composite separator, the Li/Li batteries could cycle steadily for 1000 h without noticeable dendrite growth. The LFP/Li batteries retained 63% of the discharge capacity after 1000 cycles at 1C (1.28 mA cm^{-2}) with a mass loading of 4 mg cm^{-2}.

2. Results and discussion

2.1 Design philosophy and morphology features of the PESV composite separator

The morphology and fibrous reticular microstructure of the commercial mainstream PE separator are shown in Fig. 1(a). The structure was further confirmed from the low magnification scanning electron microscopy (SEM) images shown in Fig. 1(d) and the high magnification SEM image from the top view in Fig. 1(e). The PE separator was impregnated with a mixture of rigid PSU and flexible PVDF, as depictured in Fig. 1(b), followed by scraping off the excess slurry on the PE surface and vacuum drying. The non-uniform pores in PE were filled with both PSU and PVDF, resulting in a more uniform pore size distribution.[37] Ether groups, sulfonic groups, and benzene rings in PSU endowed the PESV composite separator with high thermal stability, high intensity, and oxidation resistance,[38,39] which was confirmed from Fourier transform infrared (FTIR) spectra of PSU in Fig. 1(k). As demonstrated in Fig. 1(k), the stretching vibrations of benzene rings appeared at the characteristic peak of 1585 cm^{-1}, the asymmetric stretching vibrations of sulfonyl groups (O=S=O) were reflected at 1485 cm^{-1}, 1237 cm^{-1}, and 1015 cm^{-1} corresponding to the asymmetric stretching vibrations of aromatic ethers, respectively.[40]

Higher porosity, smaller pore size, and more uniform pore distribution were exhibited in the morphology and microstructure of the PESV composite separator, as shown in Fig. 1(c), which can be confirmed from the low-magnification SEM image shown in Fig. 1(h) and the high-magnification SEM image in Fig. 1(i). The control group is a commercial PE separator with a thickness of 16 μm, as demonstrated from the side-view SEM image shown in Fig. 1(f). The thickness of the PESV composite separator prepared by the above process is nearly the same 16 μm as shown in Fig. 1(j) and S1 (ESI†). The elemental mapping images of S and O in Fig. 1(g) and S2 (ESI†) demonstrate the successful doping and even distribution of PSU in the PE separator. The element mapping of F in Fig. S3 (ESI†) also verified the successful and uniform incorporation of PVDF into PE.

2.2 Physical properties of the PESV composite separator

A forward-looking infrared radiometer (FLIR) was used to intuitively observe and compare the morphology of the PESV and PE separators at different temperatures. As demonstrated in Fig. 2(a) and (b), the PESV composite separator could maintain the morphology integrity at 150 °C, while the commercial mainstream PE separator was deformed at 60 °C. Fig. S4 (ESI†) gives a more explicit representation, which was also proved by thermogravimetric analysis (TGA) shown in Fig. S5.† PE and

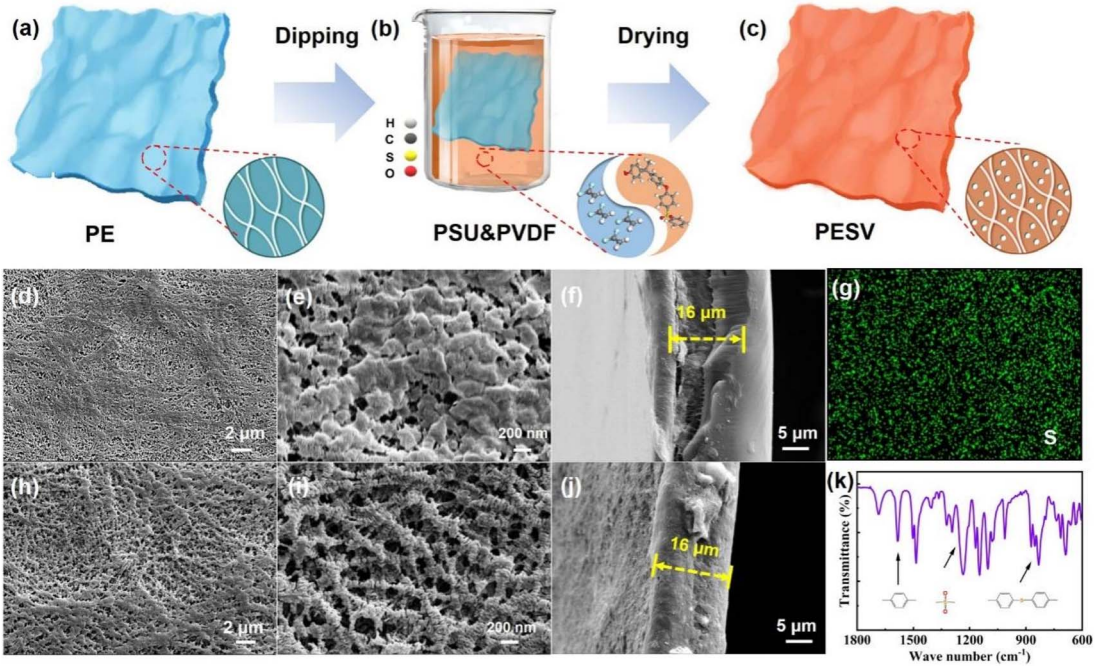

Fig. 1 Design philosophy and morphology features of the PESV composite separator. (a) Schematic of the PE separator, (b) schematic of dipping PE into the matrix of PSU and PVDF, (c) schematic of the PESV composite separator, (d) SEM graphic of PE separator from the top view with low magnification, (e) SEM graphic of the PE separator from the top view with high magnification, (f) SEM graphic of the PE separator from the side view, (g) elemental mapping image of S in a specific acreage of the PESV composite separator, (h) SEM graphic of the PESV composite separator from the top view with low magnification, (i) SEM graphic of the PESV composite separator from the top view with high magnification, (j) SEM graphic of the PESV composite separator from the side view, (k) FTIR spectrum of the PSU material.

PESV separators were heated from 25 °C to 800 °C at a rate of 10 °C per minute, and their mass changes were recorded. The PE separator showed a weight drop at 382 °C, while the PESV composite separator showed a slight weight decrease at 420 °C as depicted in Fig. S5.† The FTIR results of the PE and PESV separators are illustrated in Fig. 2(c) and S6,† respectively. A characteristic peak at 2951 cm^{-1} assigned to the stretching of C–H was observed in both PE and PESV separators.[24,41] For the PESV composite separator, characteristic peaks at 761 cm^{-1}, 871 cm^{-1}, and 974 cm^{-1} arise from the α-phase PVDF, which are also observed in FTIR results of PVDF material as demonstrated in Fig. S7 (ESI†).[42,43] The peaks at 1145 cm^{-1} and 1205 cm^{-1} result from the stretching vibration of CF_2, which appear in both the PVDF material and PESV composite separator, respectively, as depictured in Fig. 2(c) and S7 (ESI†).[25,44] The above pieces of evidence strongly confirmed the successful incorporation and stable existence of the PVDF material in the PESV composite separator. Apart from this, the peaks at 1585 cm^{-1} (benzene rings), 1485 cm^{-1} (O═S═O), 1237 cm^{-1}, and 1015 cm^{-1} (aromatic ethers) of PSU, shown in Fig. 1(k), also appeared in the PESV composite separator, implying the successful incorporation of PSU material in the PESV composite separator. PE separators are known for their high mechanical strength, but unfortunately, their lack of satisfactory resilience limits their wider use.[19,45] The strain–stress analysis was applied to research the mechanical properties of PE and PESV separators. PE could reach 78 MPa in tensile strength while the PESV composite separator achieved 104 MPa, which is attributed to the addition of the robust PSU, as demonstrated in Fig. 2(d). PE shows 102% elongation while the PESV composite separator attained 130% due to the incorporation of flexible PVDF. The desired separator was supposed to show high mechanical strength and toughness at the same time. The high mechanical strength could withstand high pressure during the battery assembly process, preventing internal short circuits caused by the penetration of the separator on the rough electrode surface. The high toughness could ensure that the performance was not affected when the battery was slightly deformed. The simple pursuit of high mechanical strength will inevitably lead to a decline in other properties of the separator such as the toughness, according to the strain–stress analysis, the mechanical strength of PESV was not improved at the expense of the toughness. The rigidity of the PSU and the toughness of PVDF endowed the PESV composite separator with both high mechanical strength and enhanced toughness.

As an amorphous polymer, PSU is partially compatible with PVDF.[39] So, the doping of PSU and PVDF will weaken the interaction between PVDF and solvent, and then affect the mechanism of separator formation and the way of pore formation. PVDF is a crystalline polymer, the crystallinity is generally about 50%, and the crystallization melting temperature is around 140 °C. Therefore, at the usual use temperature of batteries, the crystallinity of PVDF makes it difficult for molecules in the electrolyte to flow, and the charge and discharge load increase. The robust benzene ring in PSU can

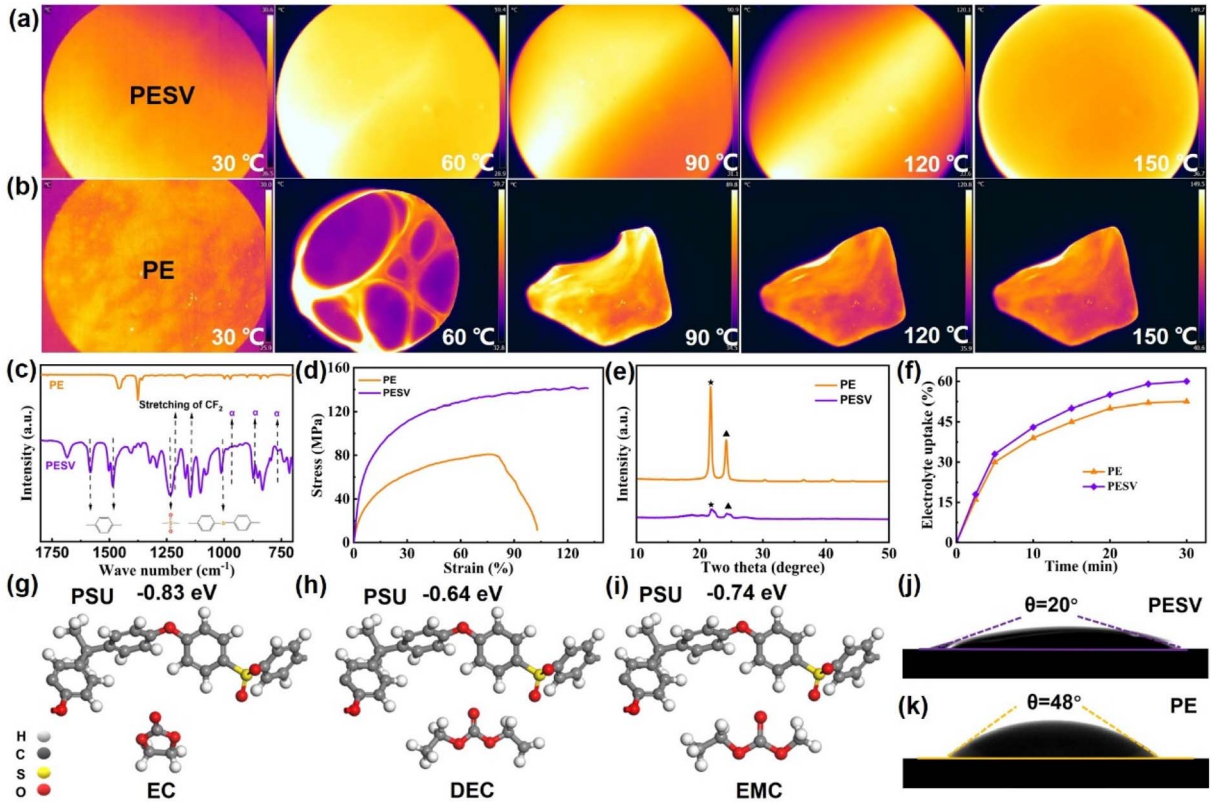

Fig. 2 Physical properties of the PESV composite separator. (a) and (b) FLIR images of the PESV and the PE separators. (c) FT-IR spectra of the PE and the PESV separators. (d) The tensile strengths of the PE and PESV separators. (e) XRD patterns of the PE and PESV separators. (f) The electrolyte uptake percentage plots of the PE and PESV separators. (g)–(i) The absorption energy of PSU with EC, DEC, and EMC, respectively. (j) and (k) The contact angles of the PESV and PE separators with the electrolyte.

promote the nucleation of PVDF and PE, decreasing the crystallinity, as demonstrated in Fig. 2(e), facilitating the transference of lithium ions in the electrolyte. Electrolyte uptake of the separators plays an essential role in the electrochemical performance of the battery.[46,47] The PE and PESV separators were immersed in the electrolyte and tested, as shown in Fig. 2(f). The electrolyte uptake of the PESV composite separator could be stabilized at 60%, while the PE was kept at 52.5%. PSU has good interaction with the commercial liquid electrolyte, which was confirmed by the absorption energy between PSU and electrolyte (ethylene carbonate, diethylene carbonate, and ethyl methyl carbonate are used to represent the electrolyte) as shown in Fig. 2(g)–(i). The adsorption energies between PSU and the electrolyte are much higher than the energies between PVDF and the electrolyte (−0.03 to −0.24 eV),[25] not to mention PE with EC, DEC, and EMC. The excellent interaction between PSU and electrolyte and hydrophilic properties of PVDF endow the PESV composite separator with a contact angle of 20° while PE shows 48°, as depictured in Fig. 2(j) and (k). Mercury porosimetry analyses were used to test the porosities of PE and PESV separators, and the results show that the PE separators had a porosity of 42%, while the PESV composite separator exhibited 65%, as demonstrated in Fig. S8 (ESI†).

2.3 Electrochemical performance of LFP/Li batteries with the PESV composite separator

The electrochemical performance was investigated by assembling LFP/Li ($LiFPO_4$ as a cathode and Li metal as an anode) batteries with PE and PESV separators, respectively. The hydrophilic PVDF endowed the PESV composite separator with more efficient transmission of Li^+ and lower transfer impedance, as demonstrated in Fig. 3(a), which were also reflected in the rate performance of the batteries, as shown in Fig. 3(b). LFP/Li batteries with the PESV composite separator delivered a higher discharge specific capacity of 154 mA h g^{-1}, 147 mA h g^{-1}, 133 mA h g^{-1}, and 104 mA h g^{-1}, while batteries with the PE separator achieved 149 mA h g^{-1}, 146 mA h g^{-1}, 129 mA h g^{-1} and 103 mA h g^{-1} at 0.5C, 1C, 3C, and 5C, respectively. Both could return to their original discharge capacities as the rate returns to 0.5C, as demonstrated in Fig. 3(b). To further research the difference in the high-rate performance of the batteries with the PESV and PE separators, high-rate cycling was implemented at 5C, as demonstrated in Fig. 3(c). The LFP/Li batteries with the PESV composite separator achieved a high specific capacity of 45.1 mA h g^{-1} with a 49% capacity retention after 100 cycles. In comparison, the LFP/Li cell with the PE separator maintained 16.8 mA h g^{-1}, retaining only 20% of the original discharge specific capacity.

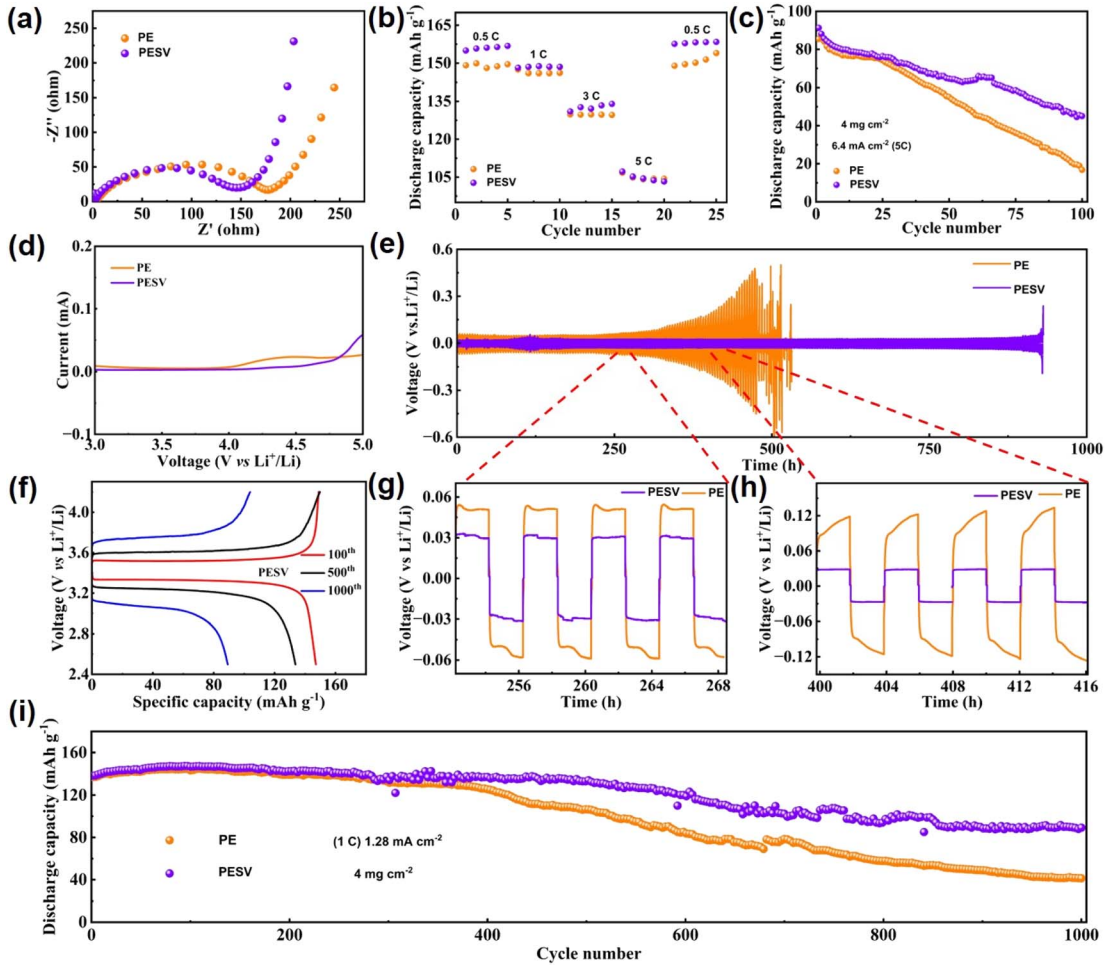

Fig. 3 Electrochemical performances of batteries with the PESV and PE separators. (a) EIS curves, (b) rate performance, (c) cycling properties at 5C (6.4 mA cm^{-2}) of batteries with the PESV and PE separators, (d) linear sweep voltammetry profiles of batteries with the PESV and PE separators, (e) the stability curves of the symmetrical Li/Li cells with the PESV and PE separators and corresponding voltage profiles at 0.5 mA cm^{-2}, (f) charging–discharging plots of batteries with the PESV composite separator, (g) the voltage–time curves of the symmetrical Li/Li batteries with the PESV and PE separator from 252 h to 268 h, (h) the voltage–time curves of the symmetrical Li/Li batteries with the PESV and PE separator from 400 h to 416 h, (i) cycling performances of cells with the PESV and PE separators at 1.28 mA cm^{-2} with mass loading of 4 mg cm^{-2}.

The separators are supposed to stay electrochemically stable for at least 4.5 V (*vs.* Li^+/Li)[30,48] as the voltage often reaches this value or even higher during the application of batteries. The stainless steel (SS)||Li batteries with the PE and PESV separators were assembled to test and make a comparison of their electrochemical oxidation window. As shown in Fig. 3(d), the voltage of the battery with the PESV composite separator sweeps up at 4.5 V (*vs.* Li^+/Li), while that of the PE separator sweeps up at 4.0 V (*vs.* Li^+/Li). The results indicate that the addition of PSU and PVDF increases the electrochemical stability of the PESV composite separator, and the inner explanations may be that the bonding energy of S=O in PSU accounts for 522 kJ mol^{-1} and C–F in PVDF accounts for 485 kJ mol^{-1}, higher than that of C–H in PE, which accounts for only 413 kJ mol^{-1}.[40] Therefore, the decomposition of PESV is more complicated than PE itself. Given the ultra-high electrochemical stability of the PESV composite separator, the symmetrical Li/Li batteries were assembled with both PE and PESV separators to further research the ability in suppressing the lithium dendrites at 0.5 mA cm^{-2}. As demonstrated in Fig. 3(e), the cell with the PESV composite separator cycles stably without noticeable current change for nearly 1000 h. Comparatively, the catastrophic short circuit occurs in the cell with the PE separator after only 400 h. For a more transparent and detailed description, the exact difference with time ranging from 252 h to 268 h and from 400 h to 416 h is intercepted and demonstrated in Fig. 3(g) and (h), respectively. The cell assembled with the PESV composite separator showed a slight overpotential of 60 mV at 0.5 mA cm^{-2}, while the cell with the PE separator achieved100 mV with time ranging from 252 h to 268 h, as shown in Fig. 3(g). As time went on, the overpotential of the cell with the PESV composite separator was maintained at 60 mV. In comparison, the overpotential of the cell with PE reached 200 mV at 0.5 mA cm^{-2} with a time ranging from 400 h to 416 h, as demonstrated in Fig. 3(h). Apart from the electrochemical stability, charge–discharge profiles of the cells with the PESV and PE separators

are shown in Fig. 3(f) and S9 (ESI†), respectively. The results demonstrate the stale charge and discharge voltage and higher capacity retention ratio of cells with the PESV composite separator.

The cycle performance of the cell is crucial among these electrochemical properties, so the cycling properties of the cell with the PESV and PE separators are characterized, as shown in Fig. 3(i). The cell with the PESV composite separator reached a discharge capacity of 89 mA h g^{-1} with 64% retention at 1.28 mA cm^{-2} with a mass loading of 4 mg cm^{-2} after 1000 cycles. In contrast, the cell with the PE separator exhibited only 41 mA h g^{-1} with 29% retention, as shown in Fig. 3(i). Also, the corresponding coulombic efficiency of batteries with various separators is demonstrated in S10 (ESI†).

2.4 Theoretical calculations on the interaction between the PESV and lithium ions

Lithium ions pass through the separator during the charging and discharging process of the battery. The truth is that the mainstream PE separator possesses an uneven pore size distribution resulting in the uneven transport of lithium ions. The long-time non-uniform deposition of lithium ions may be the dominating cause in the formation of the lithium dendrite. As demonstrated in Fig. 4(a), the formation of lithium dendrites makes the surface of lithium metal become uneven after a period of charging and discharging. In contrast, the PESV composite separator with uniform pore distribution leads to smooth charging and discharging without prominent lithium dendrite formation. To verify the above conclusions, the morphology characterization analysis is carried out on both the lithium metal anode and separator in LFP/Li batteries. After 300 cycles, the PESV composite separator still retained the intact pore distribution without obvious lithium dendrites on its surface, as illustrated in Fig. 4(b). In contrast, the surface of the PE separator became blurred due to the infiltration of electrolytes and uneven transport of lithium ions, as demonstrated in Fig. S11 (ESI†). In addition, the lithium dendrites were randomly distributed on the lithium anode surface in the LFP/Li battery with a PE separator (S12, ESI†). In contrast, no lithium dendrites were found on the surface of the lithium anode in the LFP/Li battery with the PESV composite separator, as shown in Fig. 4(c). The formation and growth of lithium dendrites bring about the continuous consumption of electrolyte and lithium metal anode, which can explain the rapid decline in the capacity of LFP/Li batteries assembled with the PE separator during long cycles. The theoretical calculations were conducted to calculate the binding energy between PSU and lithium ions at different positions in Fig. 4(d). According to the results of the operation, the maximum binding energy between PSU and lithium ions was −1.40 eV, which is higher than the binding energy between PE and lithium ions (Fig. S13†). To the totality of our best knowledge, the binding energy between polar functional groups and lithium ions is positively correlated with the uniform distribution of lithium ions.[49–51] Based on the above calculation results, PSU has a strong interaction with lithium ions, which is responsible for the uniform distribution of lithium ions.

3. Conclusion

In summary, an ultra-stable PE-based composite separator functionalized with rigid PSU and flexible PVDF was elaborately designed (abbreviated as PESV). The 16 μm PESV composite separator achieved 104 MPa, which is attributed to the addition of a rigid PSU. At the same time, the hydrophilic PVDF endowed the PESV composite separator with a contact angle of 20°. The strong binding energy between PSU and lithium ions is beneficial to the uniform distribution of lithium ions and the effective inhibition of lithium dendrite growth. Therefore, the symmetrical Li/Li batteries with the PESV performed smoothly for nearly 1000 h, while the Li/Li batteries with the PE separator only persisted for 400 h at 0.5 mA cm^{-2}. A discharge capacity retention ratio of 63% was achieved with the PESV composite separator in LFP/Li batteries at 1.28 mA cm^{-2} with a mass loading of 4 mg cm^{-2}, due to the efficient inhibition of lithium dendrites in the PESV composite separator. The series of works surrounding the PESV composite separator indicated the

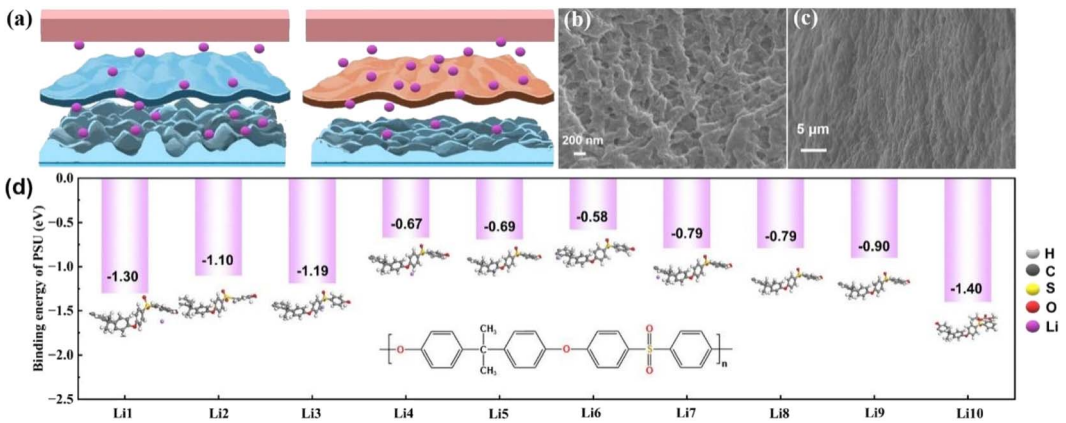

Fig. 4 Theoretical calculations on the interaction between PESV and lithium ions. (a) Schematic illustration of the LFP||Li batteries assembled with PE and PESV separators, respectively. (b) The SEM image of the PESV composite separator after 300 cycles. (c) The SEM image of lithium anode with the PESV composite separator after 300 cycles. (d) The binding energy between PSU and Li^+ at different positions.

application potential of PSU in enhancing the mechanical strength of the separator and cycling stability of batteries in the long cycle.

4. Experimental section

4.1 Materials

$LiFePO_4$, Super-P, *N*-methyl-2-pyrrolidone (NMP), and polysulfide (PSU, $M_w \sim 80\,000$) were obtained from Shanghai Aladdin Reagent Technology Co, Ltd. Polyvinylidene fluoride (PVDF, $M_w \sim 900\,000$ g mol^{-1}) was obtained from Shanghai Macklin Biochemical Co, Ltd. Aluminum (Al) foil, polyethylene (PE) separator (16 μm), and a commercial electrolyte consisting of 1.0 M $LiPF_6$ in dimethyl carbonate (EC)/diethyl carbonate (DEC)/ethylene carbonate (EMC) (volume ratio with 1 : 1 : 1) were purchased from Guangdong Canrd New Energy Technology Co., Ltd (China).

4.2 The fabrication of electrode

$LiFePO_4$, Super-P, and PVDF were mixed in a sealed glass jar with an 8 : 1 : 1 mass ratio and followed by moderate NMP addition to obtain $LiFePO_4$ cathode. The mixture was stirred appropriately at room temperature for 24 h before placing the well-mixed slurry in the clean and dried aluminum foil. The doctor blade was applied to the blade the mixture at a rate of one centimeter per second followed by vacuum drying at 80 °C overnight. The diameter of the final electrode plate was kept at 14 mm.

4.3 The fabrication of the PESV composite separator

PSU and PVDF were dissolved in NMP with a mass ratio of 1 : 1 and stirred at 80 °C in a reagent bottle for 12 h to obtain a well-mixed slurry. After cooling to room temperature, the mixed slurry was poured gently into the culture dish until the chassis was fully lined. PE separator was soaked in the slurry until translucent, accompanied by a scraper to scrap off excess surly from the surface. The obtained membrane was slowly and carefully removed and placed in a high-temperature vacuum oven at 80 °C for 12 hours. The dry composite separator was abbreviated as PESV and soaked in deionized water. Polyethylene (16 μm) was used as the control group.

4.4 The analysis of thermal stability

The diameter of the PE, and PESV separators was controlled at 19 mm, using the copper foil with the size of 5 cm × 5 cm as the baseboard. The heat was transferred from the copper foil to the separators with the temperature increasing. FLIR (A600-Series, Sweden) was used to test the heat resistance of the above separators with the infrared light ranging from 7.5 μm to 13 μm to form a photograph at 7.5 Hz.

4.5 Characterization

Scanning electron microscopy (SEM) measurements (Zeiss Supra, Germany) were used to investigate the difference in surface appearance between the PE and PESV separators. Chemical element mapping was applied to analyze the elements of the PESV composite separator. XRD (D/Max 2400, Rigaku) was used to study the crystalline structure and the difference between the PE and PESV separators at 30.0 mA and 40.0 kV with Cu Kα radiation ($\lambda = 15\,406$ Å). The surface information of these samples was studied with Fourier transform infrared spectroscopy (FTIR) (Nicolet, is50, U.S.A.). The automatic contact angle measuring instrument (Zhong Chen, JC2000D3M, China) was employed to test the contact angles on the PE and PESV separators with commercialized electrolytes. The heat endurance of the PE and PESV was analyzed using TGA (SDT 2960, USA) at a heating rate of 10 °C per minute. The electronic universal testing machine CMT6104 (MTS Systems CO. LTD.) was used to test the tensile properties of these separators. The electrolyte uptake was tested using the equation below (eqn (1))

$$(\%) = \frac{X_f - X_o}{X_o} \times 100\% \quad (1)$$

where X_o and X_f are the initial and the final masses of the separators. The thermal distribution of separators was investigated with a forward-looking infrared radiometer (FLIR-A600-Series, Sweden), and the PE and PESV separators were put on an Al foil and heated to 150 °C, respectively. In this process, the thermal distribution was recorded with the color change of the separator with an infrared camera.

4.6 Electrochemical measurement

Li symmetrical cells were charged/discharged for 2 h/2 h under the current densities of 0.5 mA cm^{-2} to investigate the galvanostatic cycling performances. Electrochemical impedance spectroscopy (EIS) was tested with LFP/Li cells to investigate the interfacial resistance. The separators were stuck in the middle of two stainless steel plates by using a CHI660 electrochemical workstation to measure the ion conductivity with the frequency ranging from 10^6 to 10^{-1} Hz.

A Li anode coupled with the as-prepared LFP cathode was used to fabricate CR2025 coin batteries to evaluate the rate and cyclic performance using the battery testing system (NEWARE, China) with a voltage range from 2.5 V to 4.2 V. The liquid electrolyte for Li/LFP cell and Li/Li cell was 1.0 M lithium hexafluorophosphate ($LiPF_6$)/ethylene carbonate (EC) + dimethyl ethylene carbonate (DEC) + ethyl methyl carbonate (EMC) electrolyte (1 : 1 : 1 vol%).

4.7 DFT calculations

For the calculation of the absorption energies and binding energy, we conducted the density functional theory (DFT) calculations as implemented in the Cambridge Sequential Total Energy Package (CASTEP). During the calculation, geometry optimization was performed using the BFGS minimization technique. The exchange–correlation energy was calculated by the generalized gradient approximation (GGA) equipped with the Perdew–Burke–Ernzerhof (PBE) functional. The energy, maximum force, and maximum displacement endowed the convergence tolerance with 1.0×10^{-5} eV per atom, 0.03 eV $Å^{-1}$,

and 0.001 Å, respectively. The absorption energy between the PSU and the electrolyte was calculated through the equation:

$$E = E_{tot} - (E_{PSU} + E_X) \quad (2)$$

in which E and E_{tot} are the adsorption energy and the gross energy of relaxed model X and model PSU in the equilibrium position, respectively. In addition, E_{PSU} represents the BFGS final energy values of model PSU, while the energy values of X molecules (X = CH_2CF_2, EC, DEC, and EMC) are renamed as E_X.

The binding energy between the PSU and Li^+ was calculated through the equation:

$$E = E_{tot} - (E_{PSU} + E_{Li^+}) \quad (3)$$

in which E and E_{tot} are the binding energy and the gross energy of the relaxed model Li^+ and model PSU in the equilibrium position, respectively. In addition, E_{PSU} represents the BFGS final energy values of PSU, while the energy values of Li^+ molecules are renamed E_{Li^+}.

Data availability

The data that support the findings of this study are available on request from the corresponding author.

Conflicts of interest

There are no conflicts to declare.

Acknowledgements

This research is supported by the Science Foundation of the National Key Laboratory of Science and Technology on Advanced Composites in Special Environments, and the National Natural Science Foundation of China (12002109). This work was sponsored by Natural Science Foundation of Chongqing, China (CSTB2022NSCQ-MSX1533, CSTC2021jcyj-msxmX10305, CSTB2022NSCQ-MSX1583, CSTB2022NSCQ-MSX1365, CSTB2022NSCQ-MSX1572, CSTB2022NSCQ-MSX0246, CSTB2022NSCQ-MSX0242, CSTB2022NSCQ-MSX0441, CSTB2022NSCQ-MSX0487, and CSTB2022TFII-OFX0034).

References

1 M. Armand and J. M. Tarascon, Building better batteries, *Nature*, 2008, **451**, 652–657.
2 G. M. Zhou, F. Li and H. M. Cheng, Progress in flexible lithium batteries and future prospects, *Energy Environ. Sci.*, 2014, **7**, 1307–1338.
3 B. Dunn, H. Kamath and J. M. Tarascon, Electrical energy storage for the grid: A battery of choices, *Science*, 2011, **334**, 928–935.
4 H. Lee, M. Yanilmaz, O. Toprakci, K. Fu and X. Zhang, A review of recent developments in membrane separators for rechargeable lithium-ion batteries, *Energy Environ. Sci.*, 2014, **7**, 3857–3886.
5 J. B. Goodenough and K. S. Park, The Li-ion rechargeable battery: A perspective, *J. Am. Chem. Soc.*, 2013, **135**, 1167–1176.
6 L. W. Dong, J. P. Liu, D. J. Chen, Y. P. Han, Y. F. Liang, M. Q. Yang, C. H. Yang and W. D. He, Suppression of polysulfide dissolution and shuttling with glutamate electrolyte for lithium sulfur batteries, *ACS Nano*, 2019, **13**, 14172–14181.
7 C. J. Orendorff, T. N. Lambert, C. A. Chavez, M. Bencomo and K. R. Fenton, Polyester separators for lithium-ion cells: Improving thermal stability and abuse tolerance, *Adv. Energy Mater.*, 2013, **3**, 314–320.
8 M. F. Lagadec, R. Zahn and V. Wood, Characterization and performance evaluation of lithium-ion battery separators, *Nat. Energy*, 2019, **4**, 16–25.
9 J. Lopez, D. G. Mackanic, Y. Cui and Z. N. Bao, Designing polymers for advanced battery chemistries, *Nat. Rev. Mater.*, 2019, **4**, 312–330.
10 B. T. Yuan, K. C. Wen, D. J. Chen, Y. P. Liu, Y. F. Dong, C. Feng, Y. P. Han, J. C. Han, Y. Q. Zhang, C. Xia, A. Sun and W. D. He, Composite separators for robust high rate lithium ion batteries, *Adv. Funct. Mater.*, 2021, **31**, 2101420.
11 T. Y. Lei, W. Chen, Y. Hu, W. Q. Lv, X. X. Lv, Y. C. Yan, J. W. Huang, Y. Jiao, J. W. Chu, C. Y. Yan, C. Y. Wu, Q. Li, W. D. He and J. Xiong, A nonflammable and thermotolerant separator suppresses polysulfide dissolution for safe and long-cycle lithium-sulfur batteries, *Adv. Energy Mater.*, 2018, **8**, 1802441.
12 S. Zhong, B. Yuan, Z. Guang, D. Chen, Q. Li, L. Dong, Y. Ji, Y. Dong, J. Han and W. He, Recent progress in thin separators for upgraded lithium ion batteries, *Energy Storage Mater.*, 2021, **41**, 805–841.
13 M. Liu, K. Turcheniuk, W. Fu, Y. Yang, M. Liu and G. Yushin, Scalable, safe, high-rate supercapacitor separators based on the Al_2O_3 nanowire polyvinyl butyral nonwoven membranes, *Nano Energy*, 2020, **71**, 104627.
14 T. W. Zhang, J. L. Chen, T. Tian, B. Shen, Y. D. Peng, Y. H. Song, B. Jiang, L. L. Lu, H. B. Yao and S. H. Yu, Sustainable separators for high-performance lithium ion batteries enabled by chemical modifications, *Adv. Funct. Mater.*, 2019, **29**, 1902023.
15 J. Y. Wan, J. Xie, X. Kong, Z. Liu, K. Liu, F. F. Shi, A. Pei, H. Chen, W. Chen, J. Chen, X. K. Zhang, L. Q. Zong, J. Y. Wang, L. Q. Chen, J. Qin and Y. Cui, Ultrathin, flexible, solid polymer composite electrolyte enabled with aligned nanoporous host for lithium batteries, *Nat. Nanotechnol.*, 2019, **14**, 705–712.
16 Y. P. Han, L. H. Ye, B. Boateng, Q. W. Sun, C. Zhen, N. Chen, X. Y. Shi, J. H. Dickerson, X. Li and W. D. He, Direct electrophoretic deposition of an ultra-strong separator on an anode in a surfactant-free colloidal system for lithium ion batteries, *J. Mater. Chem. A*, 2019, **7**, 1410–1417.
17 W. L. Sun, J. S. Zhang, M. L. Xie, D. R. Lu, Z. Zhao, Y. Q. Li, Z. Y. Cheng, S. J. Zhang and H. W. Chen, Ultrathin Aramid/COF heterolayered membrane for solid-state Li-metal batteries, *Nano Lett.*, 2020, **20**, 8120–8126.

18 S. Ali, C. Tan, M. Waqas, W. Q. Lv, Z. H. Wei, S. H. Wu, B. Boateng, J. N. Liu, J. Ahmed, J. Xiong, J. B. Goodenough and W. D. He, Highly efficient PVDF-HFP/Colloidal Alumina composite separator for high-temperature lithium-ion batteries, *Adv. Mater. Interfaces*, 2018, **5**, 1701147.

19 J. H. Dai, C. Shi, C. Li, X. Shen, L. Q. Peng, D. Z. Wu, D. H. Sun, P. Zhang and J. B. Zhao, A rational design of separator with substantially enhanced thermal features for lithium-ion batteries by the Polydopamine-ceramic composite modification of polyolefin membranes, *Energy Environ. Sci.*, 2016, **9**, 3252–3261.

20 H. Dong, P. C. Wang, S. S. Yan, Y. C. Xia, B. G. Wang, X. L. Wang and K. Liu, A thermoresponsive composite separator loaded with Paraffin@SiO_2 microparticles for safe and stable lithium batteries, *J. Energy Chem.*, 2021, **62**, 423–430.

21 X. Hao, J. Zhu, X. Jiang, H. Wu, J. Qiao, W. Sun, Z. Wang and K. Sun, Ultrastrong polyoxyzole nanofiber membranes for dendrite-proof and heat-resistant battery separators, *Nano Lett.*, 2016, **16**, 2981–2987.

22 S. Ali, C. Tan, M. Waqas, W. Lv, Z. Wei, S. Wu, B. Boateng, J. Liu, J. Ahmed, J. Xiong, J. B. Goodenough and W. He, Highly efficient PVDF-HFP/Colloidal Alumina composite separator for high-temperature lithium-ion batteries, *Adv. Mater. Interfaces*, 2018, **5**, 1701147.

23 B. Boateng, G. L. Zhu, W. Q. Lv, D. J. Chen, C. Feng, M. Waqas, S. Ali, K. C. Wen and W. D. He, An efficient, scalable route to robust PVDF-co-HFP/SiO_2 separator for long-cycle lithium ion batteries, *Phys. Status Solidi RRL*, 2018, **12**, 1800319.

24 X. Zhu, X. Jiang, X. Ai, H. Yang and Y. Cao, TiO_2 ceramic-grafted polyethylene separators for enhanced thermostability and electrochemical performance of lithium-ion batteries, *J. Membr. Sci.*, 2016, **504**, 97–103.

25 D. J. Chen, Z. Q. Zhou, C. Feng, W. Q. Lv, Z. H. Wei, K. H. L. Zhang, B. Lin, S. H. Wu, T. Y. Lei, X. Y. Guo, G. L. Zhu, X. Jian, J. Xiong, E. Traversa, S. X. Dou and W. D. He, An upgraded lithium ion battery based on a polymeric separator incorporated with anode active materials, *Adv. Energy Mater.*, 2019, **9**, 1803627.

26 Z. F. Zhou, B. B. Chen, T. T. Fang, Y. Li, Z. F. Zhou, Q. J. Wang, J. J. Zhang and Y. F. Zhao, A multifunctional separator enables safe and durable Lithium/Magnesium-sulfur batteries under elevated temperature, *Adv. Energy Mater.*, 2020, **10**, 1902023.

27 X. Li, L. X. Yuan, D. Z. Liu, M. Y. Liao, J. Chen, K. Yuan, J. W. Xiang, Z. Li and Y. H. Huang, Elevated lithium ion regulation by a "natural silk" modified separator for high-performance lithium metal anode, *Adv. Funct. Mater.*, 2021, **31**, 2100537.

28 H. Y. Huo, X. N. Li, Y. Chen, J. N. Liang, S. X. Deng, X. J. Gao, K. Doyle-Davis, R. Y. Li, X. X. Guo, Y. Shen, C. W. Nan and X. L. Sun, Bifunctional composite separator with a solid-state-battery strategy for dendrite-free lithium metal batteries, *Energy Storage Mater.*, 2020, **29**, 361–366.

29 L. Dong, Y. Liu, K. Wen, D. Chen, D. Rao, J. Liu, B. Yuan, Y. Dong, Z. Wu, Y. Liang, M. Yang, J. Ma, C. Yang, C. Xia, B. Xia, J. Han, G. Wang, Z. Guo and W. He, High-polarity fluoroalkyl ether electrolyte enables solvation-free Li^+ transfer for high-rate lithium metal batteries, *Adv. Sci.*, 2021, **9**, 2104699.

30 L. Dong, Y. Liu, D. Chen, Y. Han, Y. Ji, J. Liu, B. Yuan, Y. Dong, Q. Li, S. Zhou, S. Zhong, Y. Liang, M. Yang, C. Yang and W. He, Stabilization of high-voltage lithium metal batteries using a sulfone-based electrolyte with bi-electrode affinity and $LiSO_2F$-rich interphases, *Energy Storage Mater.*, 2022, **44**, 527–536.

31 L. Kong, Y. Wang, H. Yu, B. Liu, S. Qi, D. Wu, W. H. Zhong, G. Tian and J. Wang, In situ armoring: A robust, high-wettability, and fire-resistant hybrid separator for advanced and safe batteries, *ACS Appl. Mater. Interfaces*, 2019, **11**, 2978–2988.

32 T. Guo, J. Song, Y. Jin, Z. Sun and L. Li, Thermally stable and green cellulose-based composites strengthened by Styrene-co-Acrylate latex for lithium-ion battery separators, *Carbohydr. Polym.*, 2019, **206**, 801–810.

33 M. N. Wang, X. Chen, H. Wang, H. B. Wu, X. Y. Jin and C. Huang, Improved performances of lithium-ion batteries with a separator based on inorganic fibers, *J. Mater. Chem. A*, 2017, **5**, 311–318.

34 C. Li, S. Liu, C. Shi, G. Liang, Z. Lu, R. Fu and D. Wu, Two-dimensional molecular brush-functionalized porous bilayer composite separators toward ultrastable high-current density lithium metal anodes, *Nat. Commun.*, 2019, **10**, 1363.

35 P. Chen, Z. Wu, T. Guo, Y. Zhou, M. L. Liu, X. F. Xia, J. W. Sun, L. D. Lu, X. P. Ouyang, X. Wang, Y. S. Fu and J. W. Zhu, Strong chemical interaction between lithium polysulfides and flame-retardant polyphosphazene for lithium-sulfur batteries with enhanced safety and electrochemical performance, *Adv. Mater.*, 2021, **33**, 2007549.

36 H. Hao, T. Hutter, B. L. Boyce, J. Watt, P. Liu and D. Mitlin, Review of multifunctional separators: Stabilizing the cathode and the anode for Alkali (Li, Na, and K) metal-sulfur and selenium batteries, *Chem. Rev.*, 2022, **122**, 8053–8125.

37 L. Zhang, X. Li, M. Yang and W. Chen, High-safety separators for lithium-ion batteries and sodium-ion batteries: Advances and perspective, *Energy Storage Mater.*, 2021, **41**, 522–545.

38 B. Yu, Y. Fan, S. Mateti, D. Kim, C. Zhao, S. Lu, X. Liu, Q. Rong, T. Tao, K. K. Tanwar, X. Tan, S. C. Smith and Y. I. Chen, An ultra-long-life flexible lithium-sulfur battery with lithium cloth anode and polysulfone-functionalized separator, *ACS Nano*, 2021, **15**, 1358–1369.

39 Y. Ma, C. Dong, Q. Yang, Y. Yin, X. Bai, S. Zhen, C. Fan and K. Sun, Investigation of polysulfone film on high-performance anode with stabilized electrolyte/electrode interface for lithium batteries, *J. Energy Chem.*, 2020, **42**, 49–55.

40 Q. Cheng, Z. Cui, J. Li, S. Qin, F. Yan and J. Li, Preparation and performance of polymer electrolyte based on

Poly(vinylidene fluoride)/Polysulfone blend membrane via thermally induced phase separation process for lithium ion battery, *J. Power Sources*, 2014, **266**, 401–413.

41 T. Y. Lei, W. Chen, W. Q. Lv, J. W. Huang, J. Zhu, J. W. Chu, C. Y. Yan, C. Y. Wu, Y. C. Yan, W. D. He, J. Xiong, Y. R. Li, C. L. Yan, J. B. Goodenough and X. F. Duan, Inhibiting polysulfide shuttling with a graphene composite separator for highly robust lithium-sulfur batteries, *Joule*, 2018, **2**, 2091–2104.

42 M. Y. Li, H. J. Wondergem, M. J. Spijkman, K. Asadi, I. Katsouras, P. W. M. Blom and D. M. de Leeuw, Revisiting the delta-phase of Poly(vinylidene fluoride) for solution-processed ferroelectric thin films, *Nat. Mater.*, 2013, **12**, 433–438.

43 P. Martins, A. C. Lopes and S. Lanceros-Mendez, Electroactive phases of Poly(vinylidene fluoride): Determination, processing and applications, *Prog. Polym. Sci.*, 2014, **39**, 683–706.

44 A. C. M. de Moraes, W. J. Hyun, N. S. Luu, J. M. Lim, K. Y. Park and M. C. Hersam, Phase-inversion polymer composite separators based on hexagonal boron nitride nanosheets for high-temperature lithium-ion batteries, *ACS Appl. Mater. Interfaces*, 2020, **12**, 8107–8114.

45 M. Waqas, S. Ali, C. Feng, D. J. Chen, J. C. Han and W. D. He, Recent development in separators for high-temperature lithium-ion batteries, *Small*, 2019, **15**, 1901689.

46 S. Bag, C. Zhou, P. J. Kim, V. G. Pol and V. Thangadurai, LiF modified stable flexible PVDF-garnet hybrid electrolyte for high performance all-solid-state Li-S batteries, *Energy Storage Mater.*, 2020, **24**, 198–207.

47 W. Chen, Y. Hu, W. Q. Lv, T. Y. Lei, X. F. Wang, Z. H. Li, M. Zhang, J. W. Huang, X. C. Du, Y. C. Yan, W. D. He, C. Liu, M. Liao, W. L. Zhang, J. Xiong and C. L. Yan, Lithiophilic montmorillonite serves as lithium ion reservoir to facilitate uniform lithium deposition, *Nat. Commun.*, 2019, **10**, 4973.

48 M. S. Gonzalez, Q. Z. Yan, J. Holoubek, Z. H. Wu, H. Y. Zhou, N. Patterson, V. Petrova, H. D. Liu and P. Liu, Draining over blocking: Nano-composite janus separators for mitigating internal shorting of lithium batteries, *Adv. Mater.*, 2020, **32**, 1906836.

49 M. H. Ryou, D. J. Lee, J. N. Lee, Y. M. Lee, J. K. Park and J. W. Choi, Excellent cycle life of lithium-metal anodes in lithium-ion batteries with mussel-inspired Polydopamine-coated separators, *Adv. Energy Mater.*, 2012, **2**, 645–650.

50 W. K. Shin, A. G. Kannan and D. W. Kim, Effective suppression of dendritic lithium growth using an ultrathin coating of nitrogen and sulfur codoped graphene nanosheets on polymer separator for lithium metal batteries, *ACS Appl. Mater. Interfaces*, 2015, **7**, 23700–23707.

51 R. Zhang, X. R. Chen, X. Chen, X. B. Cheng, X. Q. Zhang, C. Yan and Q. Zhang, Lithiophilic sites in doped graphene guide uniform lithium nucleation for dendrite-free lithium metal anodes, *Angew. Chem., Int. Ed.*, 2017, **56**, 7764–7768.